Development 136, 3019-3030 (2009) doi:10.1242/dev.038174

Bicaudal C, a novel regulator of Dvl signaling abutting RNA-processing bodies, controls cilia orientation and leftward flow

Charlotte Maisonneuve[1,*], Isabelle Guilleret[1,*], Philipp Vick[2], Thomas Weber[2], Philipp Andre[2], Tina Beyer[2], Martin Blum[2] and Daniel B. Constam[1,†]

Polycystic diseases and left-right (LR) axis malformations are frequently linked to cilia defects. Renal cysts also arise in mice and frogs lacking Bicaudal C (BicC), a conserved RNA-binding protein containing K-homology (KH) domains and a sterile alpha motif (SAM). However, a role for BicC in cilia function has not been demonstrated. Here, we report that targeted inactivation of BicC randomizes left-right (LR) asymmetry by disrupting the planar alignment of motile cilia required for cilia-driven fluid flow. Furthermore, depending on its SAM domain, BicC can uncouple Dvl2 signaling from the canonical Wnt pathway, which has been implicated in antagonizing planar cell polarity (PCP). The SAM domain concentrates BicC in cytoplasmic structures harboring RNA-processing bodies (P-bodies) and Dvl2. These results suggest a model whereby BicC links the orientation of cilia with PCP, possibly by regulating RNA silencing in P-bodies.

KEY WORDS: Polycystic kidney disease, PCP, Flow, Nodal, SAM domain, K-homology

INTRODUCTION

In vertebrates, left-right (LR) asymmetry of the visceral situs is established by Nodal signals from the posterior notochord (PNC), also known as the ventral node in mammals (Brennan et al., 2002; Levin et al., 1995), Kupffer's vesicle in zebrafish, or the gastrocoel roof plate (GRP) in *Xenopus* (Essner et al., 2002; Schweickert et al., 2007). These structures extrude motile cilia, which propel a leftward fluid flow to activate Nodal by an unknown mechanism specifically on the left side (Nonaka et al., 2002; Nonaka et al., 1998) (reviewed by Shiratori and Hamada, 2006). Scanning electron microscopy analysis established that node cilia are tilted towards the posterior pole, presumably because the basal bodies are displaced from the center of the convex apical plasma membrane to the posterior hemisphere (Cartwright et al., 2004; Nonaka et al., 2005; Okada et al., 2005). Theoretical and mechanical models suggest that the posterior tilt of the rotational axes is indispensable to the coordination of effective strokes and the generation of flow (Cartwright et al., 2004; Nonaka et al., 2005; Okada et al., 2005). Confirming this prediction, irregularities in the alignment of cilia in *inv/inv* mice carrying a mutation in the ankyrin repeat protein inversin (Mochizuki et al., 1998; Morgan et al., 1998; Yokoyama et al., 1993) are accompanied by a drastic reduction in nodal flow (Okada et al., 1999; Okada et al., 2005). Consistent with a role in cilia-driven flow, inversin localizes to node cilia, and situs defects in *inv/inv* embryos can be rescued in culture by administering an artificial leftward flow (Watanabe et al., 2003). However, an inhibition of flow in theory should randomize LR asymmetry, and it is unknown why *inv/inv* mutants instead display situs inversions. To resolve this conundrum, it is crucial to validate in independent models that LR asymmetry and vectorial fluid flow in vivo are linked to the planar orientation of cilia.

Besides perturbing LR asymmetry, mutations in inversin and other ciliary proteins give rise to polycystic kidney disease (PKD), and eventually to renal failure (Benzing and Walz, 2006; Fischer et al., 2006). The hallmark of this diverse group of genetic disorders is a progressive disruption of renal tubular morphology, preceded by defects in apicobasal protein sorting and misoriented divisions of renal epithelial cells (Benzing and Walz, 2006; Fischer et al., 2006; Germino, 2005; Wilson, 2004). In the kidney, cilia act as mechanosensors that stimulate Ca^{2+} channels in response to urinary flow (Praetorius and Spring, 2003). In addition, kidney cilia harbor the atypical cadherin Fat4, a conserved regulator of planar cell polarity (PCP) that is essential to orient renal cell divisions and suppress cyst formation (Saburi et al., 2008). These findings directly link cilia to PCP. However, the mechanisms by which cilia maintain normal polarity and the tubular architecture of renal epithelial cells remain poorly understood.

Several studies suggest that cilia and associated basal bodies mediate PCP at the expense of canonical Wnt signaling (reviewed by Gerdes et al., 2009), even though loss of cilia in mice lacking intraflagellar transport proteins (IFT) other than Ift88 (Jones et al., 2008) does not generally perturb classic readouts of PCP (reviewed by Eggenschwiler and Anderson, 2007). In the canonical signaling branch, Wnt proteins bind receptor complexes of frizzled and Lrp5 or Lrp6 that are endocytosed and recruit cytoplasmic dishevelled (Dvl) to block a β-catenin destruction complex composed of axin, Apc and Gsk3β. Alternatively, to activate the PCP branch, complexes of Wnts and frizzled retain Dvl at the plasma membrane and reorganize the actin cytoskeleton by stimulating the small GTPases RhoA or Rac (reviewed by Kikuchi et al., 2009). The propagation of PCP between cells in vertebrates relies on the core PCP proteins frizzled (Fz3, Fz6 and Fz7), dishevelled (Dvl1, Dvl2 and Dvl3), prickle (Pk1 and Pk2), Van Gogh-like (Vangl1 and Vangl2), Celsr1, diversin and possibly inversin (reviewed by Simons and Mlodzik, 2008). A role for inversin is likely because

[1]Ecole Polytechnique Fédérale de Lausanne (EPFL) SV ISREC, Station 19, CH-1015 Lausanne, Switzerland. [2]University of Hohenheim, Institute of Zoology, D-70593 Stuttgart, Germany.

*These authors contributed equally to this work
[†]Author for correspondence (daniel.constam@epfl.ch)

Accepted 11 June 2009

depletion of inversin in *Xenopus* stabilizes cytoplasmic Dvl1 and thereby hyperactivates β-catenin while inhibiting polarized convergence extension movements during gastrulation (Simons et al., 2005). Similarly, the inversin-related protein diversin, an ortholog of the core PCP component Diego (Feiguin et al., 2001), promotes PCP signaling of Dvl during gastrulation, at least in part, by activating the β-catenin destruction complex (Moeller et al., 2006; Schwarz-Romond et al., 2002). When delivered ectopically to zebrafish pronephric duct, diversin can substitute for inversin to suppress renal cyst formation (Simons et al., 2005). Together, these observations led to the notion that both diversin and inversin function as a molecular switch between PCP and canonical Dvl signaling. β-catenin is also stabilized at the expense of PCP signaling during zebrafish gastrulation upon suppression of the ciliogenic kinesin Kif3a, or after depleting the basal body proteins Bbs1, Bbs4 or Mkks (Bbs6) (Gerdes et al., 2007). Similarly, mutations in ciliary (Kif3a, Ift88) or basal body proteins (Ofd) enhance Wnt/β-catenin signaling in the mouse (Corbit et al., 2008). However, the molecular machinery that links cilia to PCP remains ill-defined.

Apart from a potential role in promoting PCP, cilia themselves are also subject to regulation by PCP. Evidence that cilia respond to PCP comes from multiciliated *Xenopus* epithelial cells, in which docking of the basal bodies at the apical plasma membrane is directed by Dvl2 (Park et al., 2008), Vangl2 (Mitchell et al., 2009) and by the PCP effectors fuzzy and inturned (Park et al., 2006). It is plausible, therefore, that PCP also mediates the polarizing effect of inversin on node cilia. However, apart from inversin, no other core PCP genes are directly implicated in establishing LR asymmetry. Possibly, this is due to functional redundancy, as mild LR patterning defects of the heart, such as transposition of the great arteries and double outlet right ventricles, are observed in both *Dvl3*$^{-/-}$ mice and in *Dvl2*$^{+/-}$*;Dvl3*$^{+/-}$ compound heterozygotes (Etheridge et al., 2008). In addition, redundant activities of Dvl1 and Dvl3, and Fz3 and Fz6 have been shown to control the positioning of stereociliary bundles in the organ of Corti in the inner ear (Wang et al., 2006a; Wang et al., 2006b).

Insights into the molecular link between Wnt and cilia signaling pathways might be obtained by studying new animal models of PKD. Previous analysis of the *bpk* and *jcpk* mouse models suggests that autosomal recessive PKD (ARPKD) and autosomal dominant PKD (ADPKD)-like disease can arise as a result of mutations in *Bicc1* (Cogswell et al., 2003), the homolog of *Drosophila* Bicaudal C (BicC). BicC protein comprises three conserved K-homology (KH) domains responsible for RNA binding, and a C-terminal sterile alpha motif (SAM). *Drosophila* BicC can bind RNA in vitro and is essential in the oocyte to downregulate *oskar* mRNA at the anterior pole (Mahone et al., 1995; Saffman et al., 1998). In *Drosophila* oocytes, loss of BicC also causes mislocalization of the Epidermal Growth Factor Receptor ligand Grk, possibly because of translational deregulation of the secretory pathway (Kugler et al., 2009) or altered actin dynamics (Snee and Macdonald, 2009). However, a role for mouse BicC during axis formation has remained elusive (Cogswell et al., 2003).

Here, we assessed the function of BicC and its *Xenopus* homolog xBicC by targeted inactivation using homologous recombination in embryonic stem (ES) cells, or morpholino-mediated knockdown, respectively. Inhibition of BicC during early development perturbs the planar positioning of cilia and fluid flow in a manner reminiscent of that observed in *inv/inv* embryos, but LR asymmetry is randomized. Moreover, immunostaining of kidney cell lines revealed that BicC, through its SAM domain, assembles cytoplasmic scaffolds that harbor GFP-Dcp1a, a marker of RNA-processing bodies (P-bodies). We found that these platforms can also accommodate cytoplasmic Dvl2, and that BicC diminished the ability of Dvl2 to induce TOPFLASH, a reporter of canonical Wnt signals mediated by Gsk3β and β-catenin. Induction of TOPFLASH by LiCl, an inhibitor of Gsk3β, was unaffected, suggesting that BicC acts upstream of Gsk3β. Taken together, these results suggest that BicC mediates the alignment of node cilia, possibly by regulating the activities of Dvl and/or P-bodies. They also confirm for the first time the prediction of the flow hypothesis that the misorientation of cilia should randomize LR asymmetry.

MATERIALS AND METHODS

Gene targeting

A 2.1-kb genomic fragment of *Bicc1* comprising nucleotide 25 of exon 4 until intron 4, and a 6.0-kb *Bicc1* 3′ homology arm (intron 11-15), were used to flank a PGK-neomycin selection cassette in a targeting vector containing a thymidine kinase cassette. The *Bicc1* gene was disrupted by homologous recombination in GS-1 embryonic stem cells (gift of Michel Aguet, EPFL SV ISREC, Lausanne, Switzerland) of 129Sv/J mice. Correctly targeted ES cells were identified by PCR and validated by Southern hybridization analysis after *Hha*I digestion using 3′ and 5′ probes (Fig. S1A in the supplementary material). Germ-line chimeras were produced by blastocyst injection of selected G418-resistant clones. Mutant mice from three independent ES cell clones were phenotypically identical, in a 129Sv/J×C57Bl/6 hybrid background, and also after serial backcrossing to C56BL/6. Routine genotyping of mice was performed using the forward primers 5′-CCCAACACGGCATCTTTAGTC-3′ (complementary to intron 4) and 5′-CAGGGTCGCTCGGTGTTC-3′ (specific for the neomycin cassette), in conjunction with the reverse primer 5′-GCACGGAA-GCAGGGTTATGTC-3′ (complementary to exon 12).

Expression vectors

A full-length BicC cDNA in a CMV-SPORT6 expression vector (EST IMAGE clone 2655954) was obtained from Incyte Genomics (St Louis, MO, USA). For epitope tagging, four concatemerized *Bst*EII-HA linkers composed of oligonucleotides GTGACTATCCATATGACGTCCCAG-ATTACGCCG (sense) and ATAGGTATACTGCAGGGTCTAATGCG-GCCACTG (antisense) were inserted in tandem into a unique *Bst*EII site. The ΔKH expression vector was generated by deleting a 1233-bp *Sfo*I-*Stu*I fragment of HA-tagged BicC. The ΔSAM construct was obtained by *Eco*RI digestion and re-ligation of the BicC-HA vector. For *Xenopus* injections, untagged BicC cDNA was subcloned into the *Not*1-*Sal*1 sites of the pCS2+ vector.

Gene expression analysis

To monitor expression of the mutant *Bicc1* allele, total RNA was extracted using Trizol-LS (Invitrogen) and treated with DNase I. Both cDNA synthesis and PCR were conducted in a single tube using the SUPERSCRIPT one-step RT-PCR with Platinium Taq Kit (Invitrogen). For RT-PCR analysis, the primers 5′-GAAGGAAGCCAAAGAAATGAT-3′ and 5′-GGGCACT-CCAGACAGCAAAAT-3′ were annealed at 55°C during 40 cycles. Amplified fragments were sequenced by a commercial service (Fasteris SA, Geneva, Switzerland). Whole-mount in situ hybridization and X-gal staining of BAT-gal transgene expression were performed as described (Constam and Robertson, 2000). An antisense probe complementary to the last 1741 nucleotides of the BicC cDNA was synthesized using T7 RNA polymerase.

Histology, scanning and transmission electron microscopy

Animals or embryos were sacrificed and organs were fixed in 4% paraformaldehyde and embedded in paraffin. For scanning electron microscopy, embryos were dissected 8.0 days post coitum in Hanks balanced salt solution, fixed at room temperature for 2 hours in half Karnovsky's solution, rinsed for 10 minutes in 0.1 M Cacodylate buffer (pH 7.4) containing 10% sucrose, then incubated in ice-cold Cacodylate buffer containing 1% OsO_4. After osmification, embryos were rinsed four times in ice-cold water, then dehydrated in graded EtOH. Before critical point drying in liquid CO_2 and ion coating, embryos were soaked twice for 30 minutes in isoamyl acetate. *Xenopus* dorsal explants were prepared for SEM analysis as described

(Schweickert et al., 2007). For numerical analysis, the positioning of cilia was counted in three or four embryos in which the ventral nodes were sufficiently shallow to clearly see more than 75% of the anchoring points.

Video microscopy and image analysis

The flow of fluorescent beads (1000-fold dilution of FluoSpheres carboxylate-modified microspheres, 0.2 μm, Invitrogen) in the cavity of the PNC/ventral node was recorded for durations of 2 to 10 seconds as described (Schweickert et al., 2007) at 20 to 50 frames per second (fps) and at 20× magnification on an Axioplan 2 imaging microscope equipped with an AxioCam HSm video camera. Flow at the GRP in dorsal explants of *Xenopus* embryos was recorded as described (Schweickert et al., 2007), except that bead solution was diluted 1:2500. Cilia movements in the murine PNC/ventral node were recorded at 63-fold magnification for 2 seconds at 100 fps. To visualize trajectories, 50 frames were analyzed using ImageJ software in combination with the MTrackJ plugin (http://www.imagescience.org/meijering/software/mtrackj/).

Cell culture and transfection

HEK293T, COS1 and MDCK cells were cultured in DMEM (Sigma) supplemented with 10% fetal bovine serum (FBS, Sigma), glutamine 1% (Invitrogen) and gentamycine 1% (Invitrogen). Polarized MDCK cells were obtained after 10 days at confluence. HEK293T and MDCK cells were transfected using calcium phosphate. COS1 cells were transfected using DEAE-dextran. For stable transfection, HA-tagged BicC, ΔSAM and ΔKH constructs were subcloned into a pEF-IRESpac plasmid (Hobbs et al., 1998), and transfected into MDCK cells. Transfected cells were selected in concentrations of up to 2.5 μg/ml puromycin and expanded for 3 weeks.

Luciferase assays using the Tcf/Lef-sensitive reporter TOPFLASH

HEK293T cells were plated into 96-well dishes in triplicate at a density of 7.5×10^4 cells/well. After incubation for 24 hours, cells were transfected with TOPFLASH (0.1 μg/well) (Korinek et al., 1997) together with an identical amount of a *lacZ* expression plasmid using Lipofectamine 2000, and then incubated for 48 hours in OptiMEM medium. To measure the levels of luciferase, cell extracts were diluted 100-fold, and luminescent counts were normalized to β-galactosidase activity.

Western blot and indirect immunofluorescence analysis

Western blot was performed on extracts of cells in Laemmli buffer. Equal protein loading was confirmed by the presence of γ-tubulin. Antibodies were from Roche (rat anti-HA) or from Sigma (anti-γ-tubulin).

For immunostaining, HEK293T, COS1 and MDCK cells were grown on sterile coverslips. Expression vectors of HA-tagged BicC were transfected with KDEL-GFP (a marker of endoplasmic reticulum structures, gift from E. Snapp, Albert Einstein College of Medicine, NY, USA), Rab5-GFP or Rab7-GFP (markers of endosomes and exosomes, respectively; gifts of Marino Zerial, Max Planck Institute, Dresden, Germany), Dcp1a-GFP (a marker of P-bodies, gift of B. Seraphin, Centre de Génétique Moléculaire, CNRS Gif-sur-Yvette, France). For lysosome detection, coverslips were incubated for 30 minutes with 50 nM of LysoTracker Red (Cambrex), according to the manufacturer's protocol. Forty-eight hours after transfection, cells were fixed for 15 minutes at room temperature in 4% paraformaldehyde, washed with PBS, and permeabilized in 0.2% Triton X-100/PBS for 5 minutes. After two washes in PBS, and a 30-minute blocking step in 1% BSA/PBS, primary antibody was added for 1 hour. Rat anti-HA antibodies were purchased from Roche; mouse anti-golgin-97 from Molecular Probes, and mouse anti-Flag M2 and rabbit anti-HA from Sigma. After three washes in PBS, coverslips were incubated for 1 hour with anti-mouse Cy5, rat Cy3, rat Cy5, Alexa 563 anti-rabbit, or biotinylated anti-mouse antibodies (Jackson). To detect biotinylated secondary antibody, coverslips were rinsed three times with PBS, then incubated with streptavidine APC for 40 minutes. Stained coverslips were mounted and fluorescence was detected using a Leica Confocal Invert or Zeiss LSM510 confocal microscope. To quantify the co-distribution of cytoplasmic BicC, Dvl2 and Dcp1a, spots and surfaces were defined by peak intensity detection and thresholding using Imaris software. Spots of FlagDvl2 were considered to contact P-bodies if their centers were located at a distance of less than 0.5 μm from the Dcp1a-GFP surface that was reconstructed from *z*-stacks using Imaris software. Similarly, spots of Dcp1a-GFP and FlagDvl2 were counted as being clustered with BicC if they were less than 0.5 μm from the BicC-HA surface.

Image processing and GTT analysis

Time-lapse movies were analyzed and transformed into trajectories by ParticleTracker (Sbalzarini and Koumoutsakos, 2005) (ImageJ; http://rsb.info.nih.gov/ij/). Trajectories were processed via a custom-made script for project-R (http://cran.r-project.org/): raw data were fitted to best fit Bézier curves (iteration 10) to eliminate Brownian noise, then subjected to a Rayleigh test of uniformity, to assess the significance of the mean resultant length. Three criteria were employed to subtract trajectories suffering from Brownian movements: (1) trajectories needed to be significantly directed (Rayleigh test of uniformity); (2) trajectories had to be present for a minimum of 10-20 frames to eliminate artifacts generated during the tracking process; (3) mean velocities of beads had to exceed 2.5 μm/sec, the empirically estimated maximum speed of Brownian movement under the conditions used (Schweickert et al., 2007). Gradient time trails (GTTs) were generated as described (Schweickert et al., 2007).

RESULTS

Heterotaxia and randomization of asymmetric Nodal signaling in *Bicc1*$^{-/-}$ mice

Using whole-mount in situ hybridization, we confirmed that mouse *Bicc1* is induced throughout the PNC/ventral node between embryonic day (E) 7.5 and E8.5 (Wessely et al., 2001) (see Fig. S2 in the supplementary material). To determine the function of *Bicc1* during development, we generated a targeted allele. *Bicc1* resides on mouse chromosome 10 B5.2 and gives rise to two splice variants A and B, differing by the presence or absence of exon 21. The sequence of the longer isoform is altered in the *bpk* allele by a frame shift mutation in exon 22, leading to an ARPKD-like phenotype. By contrast, the *jcpk* mutation, a model of ADPKD, carries a point mutation in the splice acceptor of exon 3, such that exon 2 is aberrantly spliced to exon 4 (Cogswell et al., 2003). Although the resulting frame shift is expected to arrest translation, alternative initiation in exon 4, or splicing of exon 2 to exon 5, would generate a protein lacking only the KH1 domain (see Fig. S1A in the supplementary material). Because the *jcpk* and *bpk* mutations had provided no insight into potential functions of Bicc1 during early embryogenesis (Guay-Woodford, 2003), we deleted exons 5-11 of *Bicc1* by homologous recombination in ES cells (see Fig. S1B,C in

Table 1. Analysis of situs defects in *Bicc1* mutants at E13.5-E15.5

Situs:	Solitus	Inversus			Ambiguus			Total
+/+	25							25
+/–	50							50
–/–	6	10	2	1	3	3	2	27
Li/St:	n	inv	n	n	n	n	n	
Lung:	n	inv	RLI	LLI	inv	RLI	LLI	
Heart:	n	inv	n	n	inv	inv	inv	

Li, liver; St, stomach; inv, inverted; n, normal; RLI, right lung isomerism; LLI, left lung isomerism.

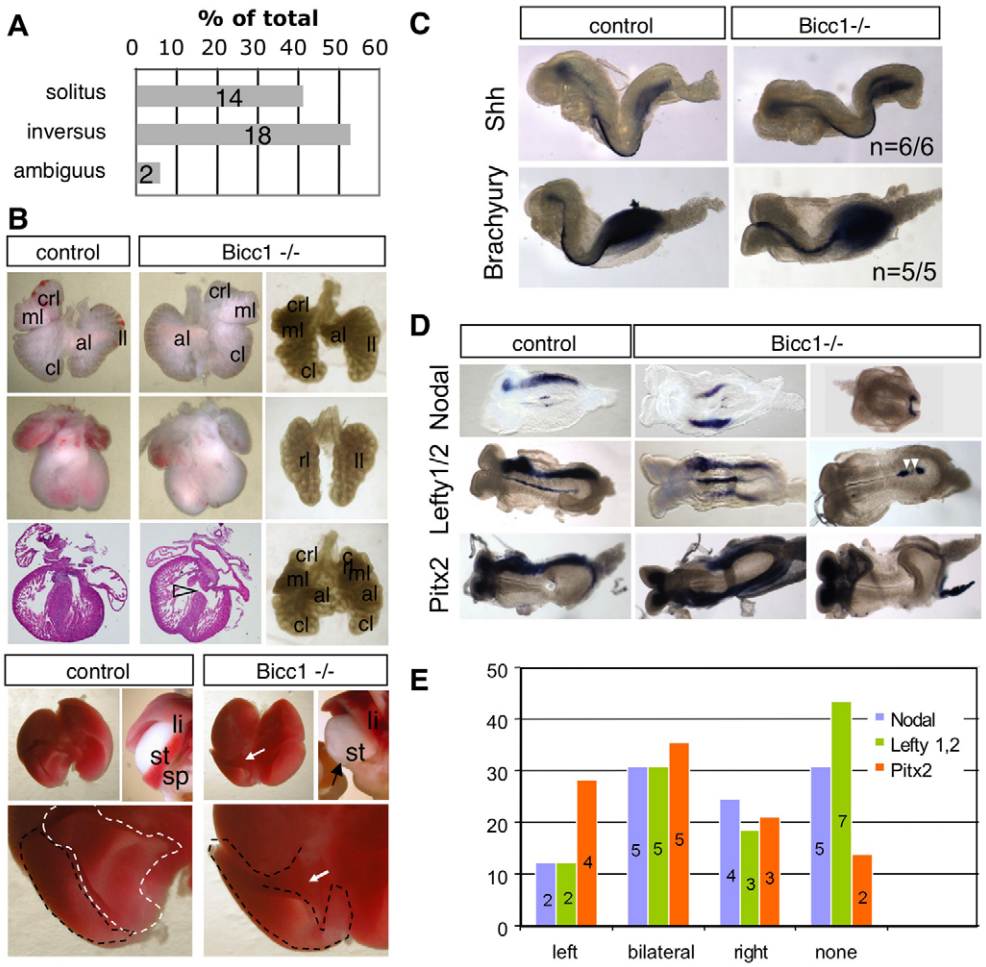

Fig. 1. LR patterning defects in *Bicc1*$^{-/-}$ mutants. (**A**) Frequency of complete situs inversions and heterotaxia (situs ambiguus) in *Bicc1*$^{-/-}$ mutants at birth. (**B**) From top to bottom: Lung, heart, liver (li)/stomach (st)/spleen (sp) of control (left) and homozygous mutants (right) at E15.5 or after birth (P2). A left-sided control stomach (st) and spleen (sp) are viewed dorsally, whereas a representative right-sided stomach of an asplenic mutant is shown from the ventral side. The right lateral and caudate lobes of a control liver are highlighted by black and white dashed lines, respectively. White arrow, absence of the caudate lobe in a left isomeric liver; open arrowhead, ventricular septal defect; black arrow, asplenia; ml, crl, al, cl, ll: medial, cranial, anterior, caudal and left lung lobes; li, liver; sp, spleen; st, stomach. (**C**) Expression of *Shh*, and *Brachyury* mRNA in the axial midline of wild-type and *Bicc1*$^{-/-}$ embryos at E8.5. n: numbers of embryos analyzed. (**D**) *Nodal* and its target gene *Pitx2* are repressed on the right side by Lefty-mediated remote feedback inhibition in the wild-type (Nakamura et al., 2006) (control). In mutants, expression of *Nodal*, *Lefty1,2* and *Pitx2* was frequently induced ectopically on the right side, but fails to normally extend in anterior direction. White arrowheads demarcate the position of the PNC. (**E**) Summary of the expression patterns of LR markers in *Bicc1* mutants. The numbers of embryos analyzed for each marker are indicated in the histogram.

the supplementary material). The deletion introduced a frameshift after K131 in exon 12, resulting in premature termination of translation. Analysis by RT-PCR and sequencing confirmed that the mutant mRNA encodes a truncated protein that comprises KH1 but terminates after K131 (see Fig. S1C in the supplementary material).

Although adult *Bicc1*$^{+/-}$ heterozygotes were healthy and fertile, only 50% of the homozygotes developed to term (see Table S1 in the supplementary material) and thereafter died within 2-15 days, apparently as a result of renal failure (data not shown). *Bicc1*$^{-/-}$ newborns frequently displayed complete situs inversions (53%, n=18/34) or situs ambiguus (6%, n=2/34; see Fig. 1A,B). During embryonic stages E13.5 to E15.5, we also detected ventricular septal heart defects (n=7/13, Fig. 1B), and situs ambiguus was more frequent (41%, n=11/27; Table 1), which is likely to account for the embryonic lethality. Besides confirming a role for BicC in kidney morphogenesis, targeted inactivation thus reveals a new function in LR axis formation.

The LR axis is patterned during early somite stages by the TGFβ family member Nodal and its feedback inhibitors Lefty1 and Lefty2 (Shiratori and Hamada, 2006). Nodal signaling is confined to the left side by a leftward fluid flow that is propelled by motile cilia in the posterior notochord (PNC), also known as ventral node (Blum et al., 2007; Hirokawa et al., 2006). Inhibition of ectopic Nodal signaling on the right side is reliant on axial midline tissues (Shiratori and Hamada, 2006). To test whether BicC is essential for midline formation, we monitored the expression of *Shh*, brachyury and *Foxa2* mRNAs in axial mesoderm and the ventral neural tube. All of these markers were expressed normally in *Bicc1*$^{-/-}$ embryos (Fig. 1C; data not shown). Nevertheless, only eight out of 47 (17%) mutants expressed *Nodal* and its target genes *Lefty1*, *Lefty2* and *Pitx2* asymmetrically on the left side. In the remaining *Bicc1*$^{-/-}$ embryos, expression in lateral plate was bilateral (15/47), inverted (10/47) or absent (14/47; see Fig. 1D,E). Interestingly, all embryos

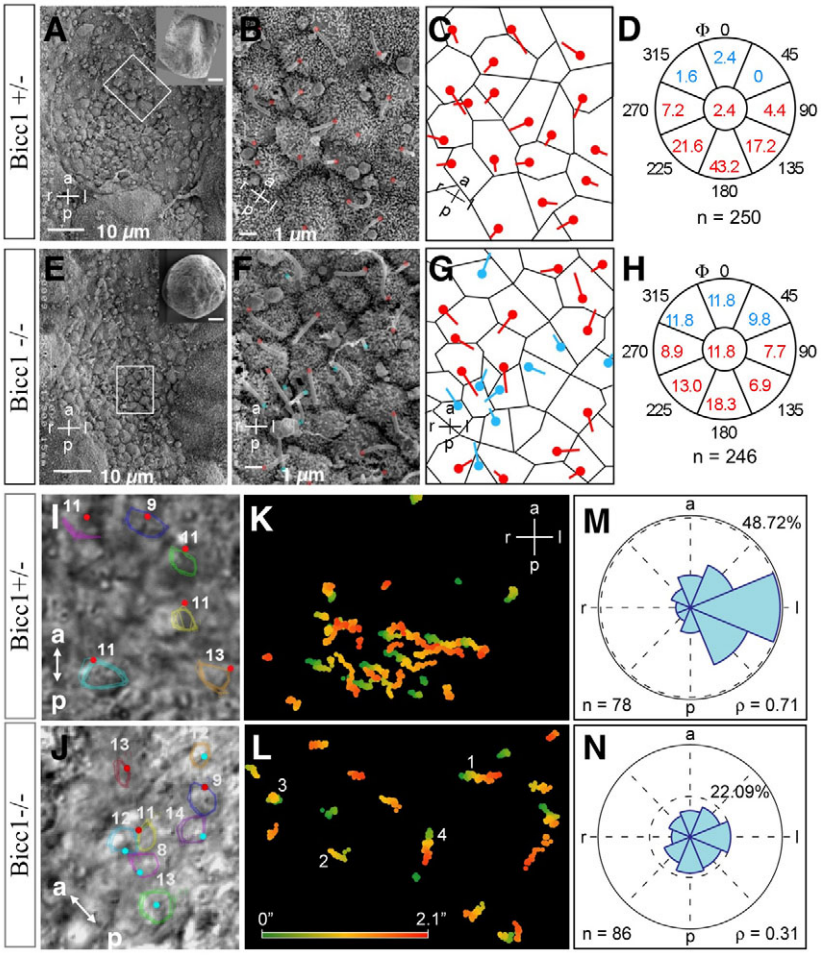

Fig. 2. Node cilia fail to respect the anteroposterior body axis in *Bicc1*$^{-/-}$ mutants. (**A-D**) Ventral node cells of control embryos. More than 80% of the cilia emanate from the three most posterior (p) octants (Nonaka et al., 2005; Okada et al., 2005). (**E-H**) In *Bicc1* mutants, 33% of the cilia are anchored in one of the three anterior octants. (A,E) Low magnifications (180×) in the inset show positioning of the embryos (a, anterior; p, posterior; l, left; r, right); intermediate magnifications (1800×) show the shape of the PNC. (B,F) Boxed areas in A and E shown at higher magnification (8000×). In B and F and the corresponding cartoons (C,G), cilia protruding posteriorly or from one of the three anterior octants are marked at their anchoring points with red or blue dots, respectively. (D,H) Percentage of cilia found in each octant or at the cell center of control (D) or mutant cells (H). The number of cilia (*n*) examined in three or four embryos (of a total of eight or ten) are indicated. (**I**) In control embryos, the trajectories (colored lines) of the tips of motile cilia are displaced posteriorly (bottom) relative to their anchoring points (red dots). (**J**) Cilia with misaligned rotational axes are marked with a blue dot at the anchoring points. Embryos in I and J were analyzed at the 2-somite stage. Numbers indicate the ciliary beating frequency (Hz); white arrows indicate the orientation of the anterior (a)–posterior (p) axis. (**K-N**) Flow analysis in representative control (K,M) and *Bicc1* mutant embryos (L,N). (K,L) Flow displayed as gradient time trails (GTTs) of 2.1-second length (cf. color gradient bar in L). Note the presence of left (1), right (2), circling (3) and posterior (4) GTTs in the *Bicc1* mutant (L) compared with the predominantly left GTTs in the control (K). (M,N) Frequency distribution of trajectory angles. Solid circles represent the 50% boundary, dashed circles mark maximum frequency in histogram specified in percent. *n*, number of particles above threshold; ρ, quality of flow.

lacking *Lefty2* mRNA in lateral plate mesoderm (*n*=7/17) instead showed ectopic expression of *Lefty1* and/or *Lefty2* behind the PNC. These results show that loss of BicC randomizes the sidedness of Nodal signaling without disrupting midline formation.

BicC is necessary to correctly orient cilia and to generate nodal flow

Next, we investigated whether laterality defects arose owing to perturbations of cilia morphogenesis or flow. Scanning electron and video microscopy analysis revealed no overt abnormalities in cilia length or motility (Fig. 2A-J, see also Movies 1, 2 in the supplementary material). However, although 82% (*n*=205/250) of cilia emanated from the posterior hemisphere in control PNC cells (Fig. 2D), this number was reduced to 38% (*n*=94/246) in BicC mutants (Fig. 2H). Thus, the majority of cilia in the mutants failed to become positioned correctly. Movies of beating cilia confirmed that the rotational axes of control cilia were tilted towards the posterior pole, whereas this polarity was perturbed in mutants (Fig. 2I,J). To assess the ability of cilia to generate flow, we recorded the movement of fluorescent beads in cultured PNC explants. Compared with the leftward flow in control embryos, flow in BicC mutants was less directed (see Movie 3 in the supplementary material) or, in a rare case (1/31), was even diverted to the right (see Fig. S3 in the supplementary material). Image analysis confirmed that trajectories in wild-type embryos were directed strictly to the left (Fig. 2K). By contrast, in BicC mutants, particles meandered considerably.

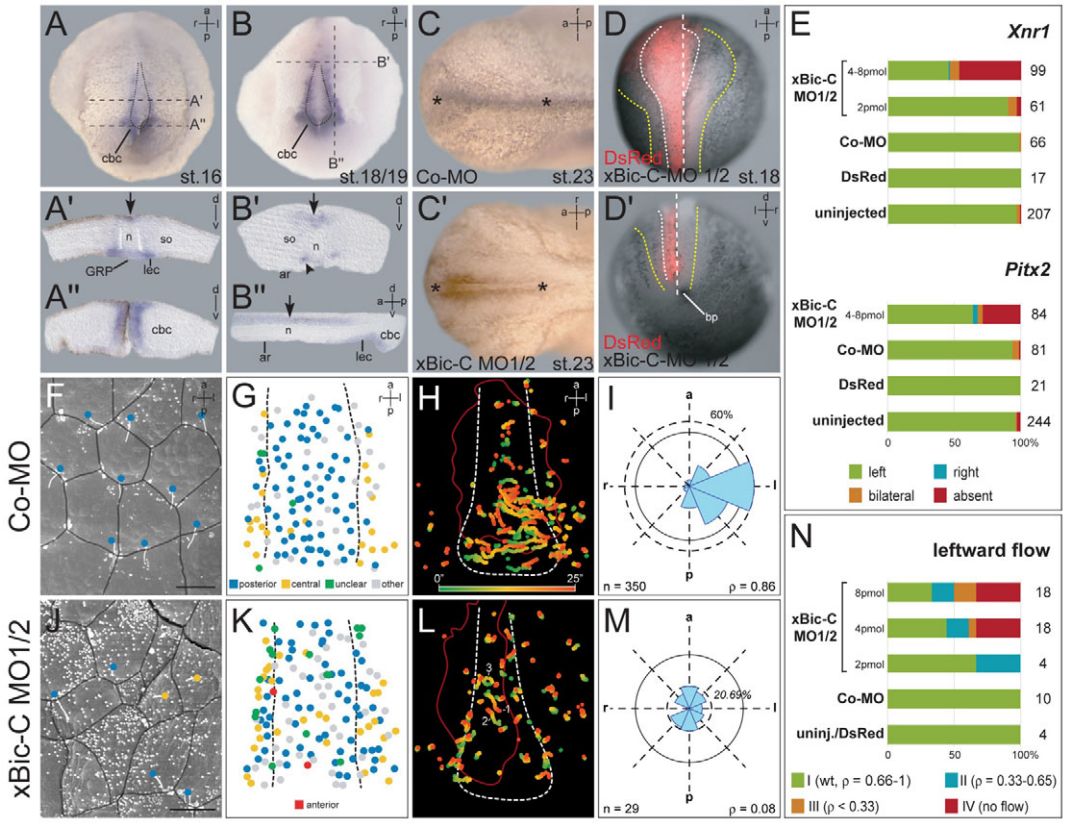

Fig. 3. Knockdown of *xBicC* alters laterality, cilia polarization and leftward flow in *Xenopus laevis*. (**A-B″**) Expression of *xBicC* in the gastrocoel roof plate (GRP; outlined by dotted lines in A and B), floor plate (arrow in A′,B′,B″) and epithelial lining of the circumblastoporal collar (cbc) at flow stages 16 (A) and 18/19 (B), as shown by whole-mount in situ hybridization analysis of dorsal explants (ventral views). Levels of sections in A′, A″, B′, B″ are indicated by dashed lines. ar, archenteron roof; n, notochord; so, somite; black arrowhead, *xBicC*- positive somitic cells. (**C**,**C′**) Neural tube closure defects in embryos injected with xBicC MO1/2 (C′) compared with Co-MO-injected specimen (C). Asterisks indicate closed (C) and open (C′) neural tubes. (**D**,**D′**) Delayed closure of the neural tube in a unilaterally injected embryo with xBicC MO1/2 and lineage tracer DsRed. Dorsal (D) and posterior (D′) view of superimposed fluorescence and bright-field images (midline indicated by dashed line, neural fold by yellow dotted line, floor plate by white dotted line). bp, blastopore. (**E**) Summary of marker gene expression patterns (*Xnr1*, top; *Pitx2*, bottom). Numbers indicate number of treated embryos. (**F**,**J**) Scanning electron microscopy analysis of GRP cells at stage 18 in Co-MO (F) and xBicC MO1/2 (J) injected embryos revealed predominantly posteriorly polarized cilia in control (F) and intermingled cilia orientation in *xBicC* morphant specimens. Scale bar: 10 μm. (**G**,**K**) Markedly reduced proportion of polarized cilia in xBicC MO1/2 (K) compared with Co-MO (G) injected embryos. The border of the GRP area relevant for flow is indicated by dashed lines. (**H**,**I**,**L**,**M**) Flow analysis in Co-MO (H,I) and xBicC MO1/2 (L,M) injected embryos. (H,L) Trajectories of beads displayed as GTTs of 25 second length (cf. color gradient bar in H). Red lines mark approximate limits of targeted areas, as visualized by co-injected DsRed; white dashed lines indicate border of the GRP. Note the presence of left (1), right (2) and circling (3) GTTs in L. (I,M) Frequency distributions of trajectory directionalities at the GRP of Co-MO (I) and xBicC MO1/2 (M) injected specimens. Solid circles represent the 50% boundary, dashed circles mark maximum frequency in histogram specified in percent. *n*, number of particles above threshold; ρ, quality of flow. Note the leftward direction of 60% of trajectories in (I) compared with the about equal distribution of trajectories in M, and the overall much reduced number of particles above the threshold of 2.5 μm/second in M. (**N**) Summary of flow analysis from 54 explants. Classification of embryos with flow into categories I-IV based on ρ. Numbers indicate the number of analyzed explants.

Individual trajectories pointed to the left, right, or were circling (Fig. 2L). The frequency distribution of trajectory angles revealed leftward movement of about 50% of control beads (Fig. 2M), whereas beads in BicC mutant embryos were transported in all directions (Fig. 2N). As a measure of flow quality, we have used ρ to describe the scattering of trajectory directions. The maximum value ρ=1 indicates that all trajectories point in the same direction, whereas a ρ-value of 0 indicates uniform distribution in all directions. Control flow such as the one displayed in Fig. 2K reached a ρ-value of 0.71, whereas the BicC mutant flow was characterized by a ρ-value of 0.31 (Fig. 2L,N). Together, these results demonstrate that BicC is necessary to align the tilt of PNC cilia with the anteroposterior body axis as a prerequisite of leftward flow and LR axis formation.

A role for BicC in generating cilia-driven flow is conserved in *Xenopus*

To quantitate flow dynamics, we depleted xBicC in *Xenopus* embryos, which can be analyzed in large numbers using advanced automated software tools (Schweickert et al., 2007). During flow stages (stages 16-19), *xBicC* was expressed in the gastrocoel roof plate (GRP), the floor plate, and the epithelial lining of the circumblastoporal collar (Fig. 3A,B), consistent with a conserved role for xBicC in regulating flow. To deplete xBicC in the GRP and floor plate, the morpholino oligonucleotides xBicC MO1 and MO2 (Tran et al., 2007) were injected into the marginal zone of four-cell embryos (Blum et al., 2009). If xBicC MO1/2 was injected on both sides (Fig. 3C,C′) or unilaterally (Fig. 3D,D′),

neural tube closure between stages 12-24 was delayed. Therefore, to analyze the left-sided marker genes *Xnr1* and *Pitx2*, injected embryos were cultured until stages 22-34. Embryos injected with DsRed mRNA or a control morpholino oligonucleotide (Co-MO) revealed normal left-sided gene expression patterns (Fig. 3E; see also Table S2 in the supplementary material). By contrast, injection of xBicC MO1/2 dose-dependently perturbed gene expression patterns in 20-60% of cases (Fig. 3E; see also Table S2 and Fig. S4 in the supplementary material). To elucidate the cause of LR asymmetry defects, xBicC morphants and controls were analyzed by scanning electron microscopy at stage 17/18. In representative control embryos, these stages were characterized by about 75% (71/94) of cilia being tilted towards the posterior pole in the flow-relevant areas (dotted lines) of wild-type GRPs (Schweickert et al., 2007) (Fig. 3F,G). By contrast, in xBicC morphants, posteriorly polarized cilia were reduced in number to less than 50% (40/83), with the percentage of misaligned cilia rising accordingly (Fig. 3J,K). These results suggest a conserved role for xBicC in aligning the planar polarity of ciliated cells with the anteroposterior body axis.

To monitor flow, dorsal explants of control- and MO-injected embryos were analyzed by adding fluorescent beads (see Movie 4 in the supplementary material). For the evaluation of flow, trajectories were selected that were directed and that exceeded the empirically selected threshold of maximum Brownian movement. Explants were grouped into four categories on the basis of flow phenotype. Category I represented robust leftward flow (ρ=0.66-1); category II (ρ=0.33-0.65) and category III (ρ<0.33) mildly and severely affected flow, respectively (see Fig. S5 in the supplementary material). If less than 25 particles per movie displayed velocities of >2.5 μm/sec (i.e. above threshold), embryos were classified as category IV (no flow). Trajectories of individual beads were generated by automated computation of gradient time trails (GTTs) (Schweickert et al., 2007). In representative control specimens (category I), a robust leftward flow was evident by the straight direction of trajectories towards the left (Fig. 3H). By contrast, beads in the GRP of representative xBicC morphants (category III) were frequently trapped by non-polarized cilia, resulting in non-directional, meandering trails (Fig. 3L, see also Movie 4 in the supplementary material). The frequency distribution of trajectory angles above the GRP, and the ρ values for flow in explants from xBicC morphants clearly differed from that in controls (Fig. 3I,M,N). Furthermore, the effects of xBicC MO1/2 were dose dependent, and a clear correlation between LR marker gene expression patterns and flow categories was obvious (compare Fig. 3E with 3N), confirming that altered gene expression resulted from aberrant flow.

The SAM domain recruits BicC to the periphery of P-bodies and downregulates BicC protein levels in polarized MDCK cells

Homologs of BicC in *Drosophila* and nematodes are implicated in regulating the localization or translation of target mRNAs (Chicoine et al., 2007; Eckmann et al., 2002; Mahone et al., 1995). To determine how BicC might regulate target genes, we visualized the subcellular localization of tagged BicC and truncated mutant forms lacking the KH- or SAM domains. Immunostaining of transfected HEK293T cells and confocal imaging detected BicC in discrete cytoplasmic foci that do not overlap with molecular markers of the ER, Golgi, endosomes or lysosomes (see Fig. S6 in the supplementary material). BicC formed similar structures in transfected COS1 cells (Fig. 4A).

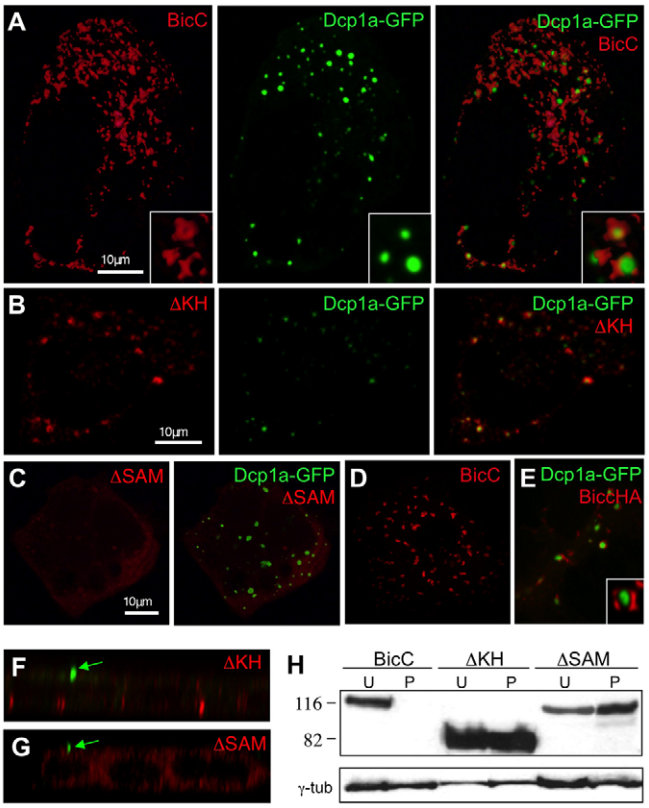

Fig. 4. The SAM domain assembles BicC in scaffolds accommodating P-bodies. (**A**) Localization of HA-tagged BicC in COS1 cells. To visualize how BicC (red) accommodates the P-body marker Dcp1a-GFP (green), the red surface in A was reconstructed from *z*-stacks. (**B**,**C**) Confocal imaging of truncated ΔKH reveals a similar distribution (B), whereas ΔSAM stained diffusely. (**D**,**E**) Unpolarized MDCK cells expressing BicC alone (D) or with Dcp1a-GFP. A deconvoluted confocal section (inset in E) shows that Dcp1a-GFP is sandwiched by BicC. (**F**,**G**) In polarized MDCK cells, neither ΔKH nor ΔSAM (red) colocalize with acetylated tubulin (green) in cilia. (**H**) Western blot analysis of unpolarized (u) or polarized (p) MDCK cells stably transfected with full-length Bicc1, ΔKH or ΔSAM. Upon cell polarization, the expression of full-length BicC drops below detectable levels.

Reconstruction of the 3D surface indicated that BicC foci formed tube- and vesicle-like structures around or adjacent to P-bodies that were marked by a GFP fusion of the decapping enzyme Dcp1a (Cougot et al., 2004) (Fig. 4A). In representative cells (n=10), 51±26% of the Dcp1a-GFP spots were at least partially coated by BicC-HA. A similar distribution was observed for mutant BicC lacking the KH domains (ΔKH, Fig. 4B), whereas deletion of the SAM domain gave rise to a diffuse cytoplasmic staining (Fig. 4C). Similarly in MDCK kidney epithelial cells, BicC and ΔKH localized in cytoplasmic foci, whereas ΔSAM staining was diffuse (Fig. 4D-G; data not shown). When MDCK cells expressing BicC were differentiated into fully polarized, ciliated epithelial cells (Fig. 4F,G, arrow), full-length BicC failed to accumulate, indicating that the combination of the KH and SAM domains negatively regulates BicC protein translation or stability under the conditions examined (Fig. 4H). Altogether, these experiments show that BicC is recruited to the periphery of P-bodies in a SAM domain-dependent manner.

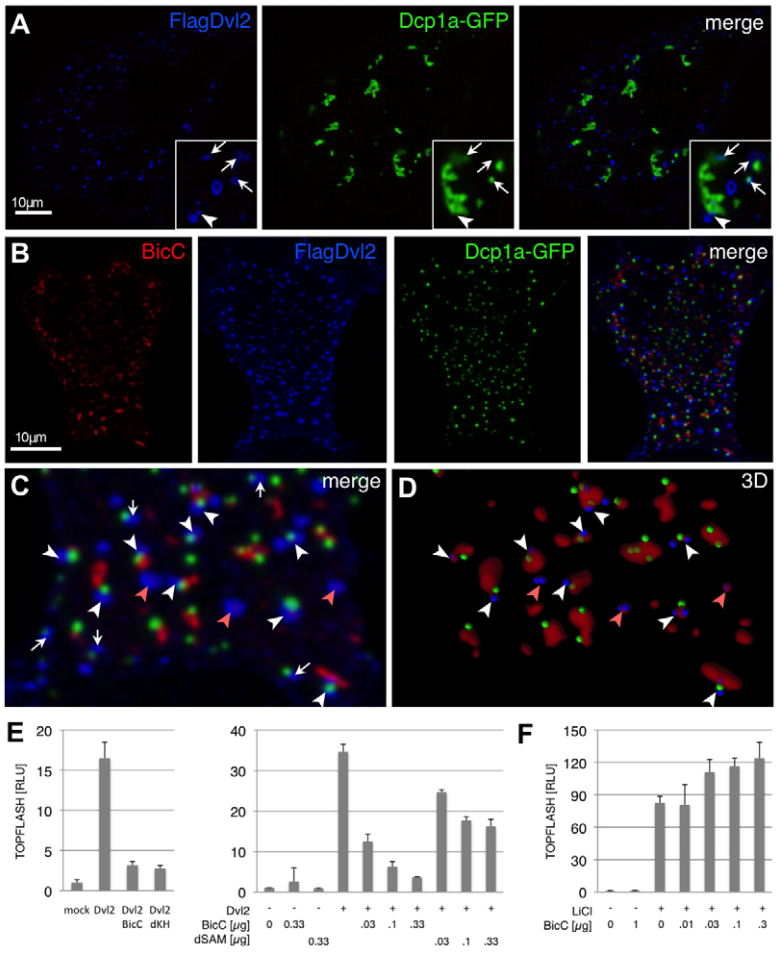

Fig. 5. Interactions of BicC with cytoplasmic Dvl2 signaling platforms. (**A**) Distribution of FlagDvl2 (blue) and Dcp1a-GFP (green). Arrows in insets highlight areas of overlap. (**B-D**) Triple fluorescence analysis of BiccHA (red), FlagDvl2 (blue) and Dcp1a-GFP (green) in individual and merged channels (B). Higher magnification of a confocal section (C) combined with a 3D reconstruction of the BiccHA surface (D) reveals clustering of FlagDvl2 with BicC (red arrowheads) or with Dcp1a-GFP (white arrows), or with both (white arrowheads). For clarity, the centers of green and blue staining in proximity (<0.5 μm) of the BiccHA surface in F are represented by spots. (**E**,**F**) BicC dose-dependently inhibits induction of the TOPFLASH reporter by Dvl2 in transfected HEK293T kidney cells, and this inhibition was severely compromised in ΔSAM, but not in ΔKH (E). By contrast, induction of TOPFLASH by LiCl was unaffected or even slightly enhanced by BicC (F). Similar results were obtained in three independent experiments.

BicC inhibits Dvl signaling in the canonical Wnt pathway

Dvl, a positive regulator of the canonical Wnt pathway has been shown to multimerize in similar structures. (Bilic et al., 2007; Schwarz-Romond et al., 2007a; Schwarz-Romond et al., 2005). Prompted by our observations, we assessed whether Dvl and BicC would colocalize in cytoplasmic punctae. Consistent with previous reports, FlagDvl2 was detected in discrete puncta that arise by multimerization via the DIX domain (Schwarz-Romond et al., 2007a; Schwarz-Romond et al., 2007b). Interestingly, in Dvl2-expressing cells, P-bodies formed irregularly shaped clusters and, among 28±11 Dcp1a-GFP surfaces examined per cell (n=9), 7±3 (38±20%) abutted FlagDvl2 puncta (Fig. 5A). In cells co-expressing FlagDvl2 and BicC-HA, P-bodies remained dispersed, and, of those occupied by FlagDvl2 (40±9% of n=451 in seven cells), 60±7% cuddled to the BicC-HA surface (Fig. 5B-D). Furthermore, 35±6% of the FlagDvl2 puncta far from P-bodies (n=516/695 in seven cells) were at the BicC-HA surface (Fig. 5C,D, red arrowheads). To determine whether BicC directly interacts with Dvl2, transfected COS1 cells were analyzed by co-immunoprecipitation. Neither BicC nor ΔKH pulled down FlagDvl2, and their overexpression did not deplete FlagDvl2 (see Fig. S7 in the supplementary material). However, BicC dose-dependently inhibited FlagDvl2-mediated induction of TOPFLASH, a reporter of canonical Wnt signaling (Fig. 5E). This inhibitory effect was reduced upon deletion of the SAM domain, indicating that concentration in cytoplasmic foci is important. By contrast, the activity of ΔKH was similar to that of wild-type BicC. Furthermore, BicC failed to diminish induction of TOPFLASH by LiCl (Fig. 5F), indicating that BicC blocks signaling of Dvl upstream of Gsk3β. Taken together, these results suggest that BicC, via its SAM domain and independently of its KH domains, is concentrated in cytoplasmic platforms that inhibit canonical Dvl2 signaling.

To monitor the influence of BicC on the canonical Wnt pathway in vivo, *Bicc1* mutants were crossed with transgenic BAT-gal reporter mice, which express a *lacZ* reporter of β-catenin/TCF signaling (Maretto et al., 2003). Whole-mount staining of BAT-gal embryos at E7.5-E8.0 showed that *lacZ* expression is reduced in the PNC compared with the adjacent primitive streak region in *Bicc1* wild-type embryos, and that this local down-modulation of BAT-gal is impaired in the PNC of *Bicc1*$^{-/-}$ embryos (n=6/7; Fig. 6A), indicating that BicC attenuates canonical Wnt activity in the posterior notochord.

DISCUSSION

This study reveals a conserved role for BicC in directing the planar orientation of cilia and leftward fluid flow during LR axis formation that has not been described in *bpk* and *jcpk* mice. Thus, our new *Bicc1* allele unequivocally confirms for the first time the prediction of the flow hypothesis that misorientation of PNC cilia should randomize LR asymmetry. Furthermore, we have shown that the SAM domain concentrates BicC in cytoplasmic tube- and vesicle-like structures harboring P-bodies and cytoplasmic Dvl2, and that BicC inhibits Dvl2 signaling via the canonical β-catenin/TCF

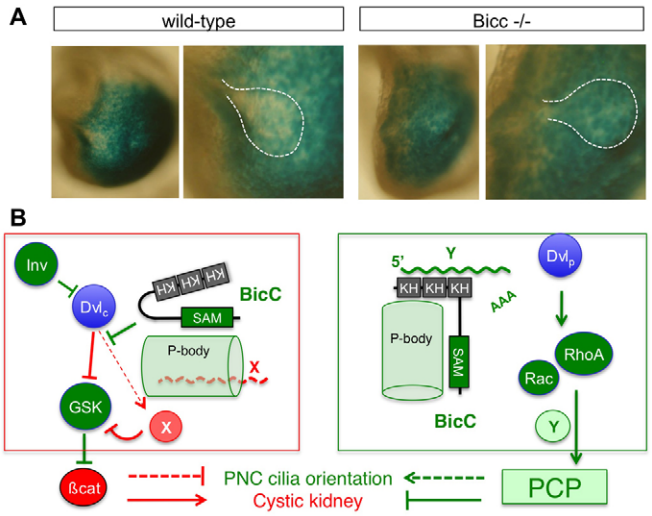

Fig. 6. Regulation of Dvl signaling by BicC. (**A**) Expression of the BAT-gal reporter of β-catenin/TCF signaling in wild-type and Bicc1$^{-/-}$ embryos at E7.75. Dashed lines in the high magnification images indicate the periphery of the ventral node. (**B**) Dvl proteins in the cytoplasm (c) or at the plasma membrane (p) transduce canonical and non-canonical Wnt signals through β-catenin (βcat) or the small GTPases (RhoA or Rac), respectively. (Red box, left) Dvl$_c$ inhibits Gsk3β in the β–catenin destruction complex through an unknown mechanism that is blocked by BicC. Unlike inversin (Inv), BicC inhibits Dvl without triggering its degradation. Inhibition of Dvl$_c$ involves the SAM domain, which concentrates BicC in structures abutting P-bodies. By interacting with CCR4 deadenylase (Chicoine et al., 2007) and/or P-bodies, BicC may stimulate degradation of an mRNA encoding a Gsk3β inhibitor (X). Also Dvl2 can cluster with P-bodies, but its potential to regulate RNA silencing (dashed red line) is unknown. (Green box, right) In addition, BicC protein possibly sequesters associated mRNAs outside P-bodies and delays their degradation after deadenylation (AAA); for example, to promote the synthesis of an agonist (Y) of PCP signal transduction. The proteins X and Y, and the interactions represented by the dashed lines are hypothetical. Components that promote or antagonize PCP signaling are depicted in green or red, respectively.

pathway. Based on these results, we propose that BicC links cilia orientation to PCP signals, possibly by counteracting Dvl-induced activation of β-catenin.

In *bpk* mice, a point mutation disrupting one of the two splice variants of *Bicc1* causes ARPKD, whereas *jcpk* mice carry a dominant mutant allele associated with an ADPKD-like phenotype (Cogswell et al., 2003). Our targeted mutation leads to a randomization of visceral tissue positioning, combined with a cystic phenotype in newborn kidney and pancreas that will be described elsewhere (I.G., unpublished observation). Transcription of this new allele might give rise to a truncated N-terminal peptide of 131 amino acids comprising the first KH domain. However, LR patterning and kidney defects are not observed in heterozygotes, suggesting that a gain-of-function is unlikely to account for LR defects. Corroborating this conclusion, morpholino-mediated knockdown confirmed that a homolog of BicC is also required for LR axis formation in *Xenopus*.

LR asymmetry is specified by Nodal activity, which is symmetrically induced in the PNC by the Notch pathway (Brennan et al., 2002; Krebs et al., 2003; Raya et al., 2003), but is then biased by leftward flow to signal preferentially on the left side (Nonaka et al., 2002). Flow generation is thought to depend on the posterior tilting of node cilia (Cartwright et al., 2004; Nonaka et al., 2005; Okada et al., 2005). Consistent with this model, inhibition of flow in *Bicc1* mutants was accompanied by a decrease in the number of correctly oriented cilia from 80% to 38%. A similar cilia misorientation phenotype has only been described in *inv/inv* mice (Okada et al., 2005). Even though cilia fail to align parallel to the anteroposterior axis, they remain fully motile and thus counteract the leftward fluid flow in both *inv/inv* and *Bicc1*$^{-/-}$ embryos. However, the outcome differs between these mutants. Poor flow in *Bicc1* mutants leads to situs randomization. By contrast, cilia malpositioning in *inv/inv* embryos is associated with situs inversions (Yokoyama et al., 1993). Although depletion of inversin can also randomize heart positioning in zebrafish, other aspects of LR asymmetry or cilia positioning have not been analyzed in that model (Otto et al., 2003). The present observations thus indicate that the *inv/inv* mutation probably has some additional function besides perturbing the planar orientation of cilia.

In zebrafish pronephros, depletion of inversin leads to cystic growth (Otto et al., 2003), which can be suppressed by injecting diversin, an ortholog of the core PCP protein Diego (Simons et al., 2005). Inversin selectively sequesters the cytoplasmic, but not the membrane-bound pool of Dvl1, suggesting that it promotes PCP by inhibiting the activity of Dvl in the Wnt/β-catenin pathway. Consistent with this model, hyperactivation of β-catenin signaling is sufficient to trigger cystic growth in the kidney of transgenic mice (Qian et al., 2005; Saadi-Kheddouci et al., 2001). However, whether an imbalance between PCP and Wnt/β-catenin signaling in *inv/inv* mutants also accounts for the misorientation of node cilia during LR axis formation is not known.

To assess whether BicC regulates Wnt signaling, we explored interactions between BicC and Dvl. We have shown that BicC downregulates expression of the BAT-gal reporter transgene in the PNC/ventral node, and that it can inhibit β-catenin/TCF signaling induced by Dvl2 in TOPFLASH reporter assays. By contrast, BicC failed to inhibit the induction of TOPFLASH by LiCl. Immunostaining showed that BicC forms cytoplasmic platforms, which accommodate foci of Dvl2 previously associated with canonical Wnt signaling (Bilic et al., 2007; Schwarz-Romond et al., 2007a; Schwarz-Romond et al., 2005). These observations suggest that BicC attenuates canonical Wnt signaling at the level of Dvl. Furthermore, whereas inversin directly inhibits canonical Wnt signals by depleting Dvl1 (Simons et al., 2005), BicC did not significantly reduce the levels of Dvl2. Thus, BicC is likely to act in parallel to inversin to align cilia in response to PCP cues (Fig. 6B). PCP signaling is also required for neural tube closure (Wallingford and Harland, 2002). Whereas neural tube closure is impaired in xBicC-depleted *Xenopus* embryos, this and other readouts of PCP, such as eyelid closure and hair follicle orientation in the skin, were normal in *Bicc1*$^{-/-}$ mice. Also, convergence-extension movements during gastrulation appeared normal, confirming that BicC is not a core PCP protein. However, we do not rule out the possibility that a subtle PCP defect contributes to the failure of Lefty1-expressing cells in the midline to colonize the ventral neural tube (Brennan et al., 2002).

Dvl proteins must localize to the plasma membrane for PCP signaling, whereas the canonical Wnt pathway relies on a cytoplasmic pool of Dvl aggregating with axin during or after endocytosis of Lrp6 (Bilic et al., 2007; Kikuchi et al., 2009; Wallingford and Habas, 2005; Yamamoto et al., 2006). Although the activities of these distinct pools of Dvl antagonize each other (for a review, see Wallingford and Habas, 2005), the mechanisms

regulating pathway selection are poorly understood. Recent studies in zebrafish revealed that Dvl interacts with seahorse, a novel regulator of LR asymmetry and renal morphogenesis also known as leucine rich repeat containing 6 (Lrrc6), and that seahorse reduces the induction of Wnt/β-catenin target genes during gastrulation (Kishimoto et al., 2008). In addition, a genome-wide screen in *Drosophila* cells recently showed that PCP signaling depends on an association of Dvl with negatively charged phospholipids in the plasma membrane, and that this interaction is facilitated by a reduction of the intracellular pH by the sodium proton exchanger Nhe2 (Simons et al., 2009). It might be interesting, therefore, to assess in future studies whether canonical Wnt signals antagonize the expression or activity of Nhe2.

Here, we have directly demonstrated for the first time that BicC, through its SAM domain, forms cytoplasmic structures that can accommodate P-bodies and Dvl2. P-bodies are key regulators of mRNA surveillance, degradation, translational repression and RNA-mediated gene silencing (Cougot et al., 2004; Eulalio et al., 2007), but to our knowledge, they are not implicated in transmitting canonical Wnt signals. Our finding that the SAM domain promotes both BicC localization and the inhibition of Dvl2 indicates that P-bodies probably must at least communicate with BicC. In one possible scenario, BicC could mediate translational silencing of a Gsk3 inhibitor X by P-bodies (Fig. 6B, left box). The recent findings that β-catenin can be released from Gsk3β by the RNA helicase activity of p68 (Yang et al., 2006), and that p68 activates the *let-7* miRNA precursor are consistent with such a model (Salzman et al., 2007). Alternatively, or in addition, BicC might promote PCP by blocking a direct inhibition of Gsk3β by Dvl2, the mechanism of which is currently unknown.

In *Drosophila* oocytes, BicC confines Oskar expression to the posterior pole to promote anterior cell fates (Mahone et al., 1995; Saffman et al., 1998). Posterior localization of *oskar* mRNA also depends on the Dcp1a homolog Dcp1 (Lin et al., 2006), which has been detected in cytoplasmic foci of *Drosophila* oocytes and nurse cells together with Maternal Expression at 31B (Me31B) (Lin et al., 2006). Me31B, the homolog of the yeast decapping activator Dhh1p, is localized to cytoplasmic foci by *Drosophila* BicC, apparently through a direct interaction (Chicoine et al., 2007; Kugler et al., 2009). *Drosophila* BicC has also been shown to repress translation of its own mRNA by recruiting the NOT3/5 component of the CCR4 deadenylase complex (Chicoine et al., 2007). CCR4 (also known as Twin) shortens the poly A tail length of *oskar* mRNA (Benoit et al., 2005), and in mammalian cells it stimulates the assembly of P-bodies (Andrei et al., 2005; Cougot et al., 2004; Zheng et al., 2008). These observations are consistent with our model that BicC regulates translational silencing of target mRNAs in P-bodies. However, we do not exclude that besides inhibiting cytoplasmic Dvl, BicC promotes PCP through additional mechanisms (Fig. 6B, right box). It will be interesting to determine in future studies the function of the novel P-body microenvironment defined by BicC, and whether BicC is needed to correctly canalize a response to Wnt signals at the level of RNA silencing.

Acknowledgements

We are grateful to Friedrich Beermann for blastocyst injections, to Olav Zilian and Nadav Ben Haim for technical advice, and to Christophe Fuerer for critical reading of the manuscript. GFP-Dvl2 and FlagDvl2 expression vectors were kindly provided by Marianne Bienz, and Dcp1a-GFP by Bertrand Séraphin. BAT-gal transgenic mice were a kind gift of Stefano Piccolo. We also thank Gisèle Ferrand and her staff at the ISREC animal facility for animal care, Oliver Wessely for sharing xBicC morpholinos and plasmids, Dr Nobutaka Hirokawa for the protocol to fix cilia, Michel Bonin and Antonio Mucciolo for the SEM analysis of mouse embryos, and Werner Amselgruber for access to his SEM in Hohenheim. This project has been supported by Oncosuisse (grant SKL 1101-02-2001) and the PKD Foundation (grant 151a2r) to D.B.C., and by DFG grants to M.B.

Competing interests statement

The authors declare that they have no competing financial interests.

Supplementary material

Supplementary material for this article is available at http://dev.biologists.org/cgi/content/full/136/17/3019/DC1

References

Andrei, M. A., Ingelfinger, D., Heintzmann, R., Achsel, T., Rivera-Pomar, R. and Luhrmann, R. (2005). A role for eIF4E and eIF4E-transporter in targeting mRNPs to mammalian processing bodies. *RNA* **11**, 717-727.

Benoit, B., Mitou, G., Chartier, A., Temme, C., Zaessinger, S., Wahle, E., Busseau, I. and Simonelig, M. (2005). An essential cytoplasmic function for the nuclear poly(A) binding protein, PABP2, in poly(A) tail length control and early development in Drosophila. *Dev. Cell* **9**, 511-522.

Benzing, T. and Walz, G. (2006). Cilium-generated signaling: a cellular GPS? *Curr. Opin. Nephrol. Hypertens.* **15**, 245-249.

Bilic, J., Huang, Y. L., Davidson, G., Zimmermann, T., Cruciat, C. M., Bienz, M. and Niehrs, C. (2007). Wnt induces LRP6 signalosomes and promotes dishevelled-dependent LRP6 phosphorylation. *Science* **316**, 1619-1622.

Blum, M., Andre, P., Muders, K., Schweickert, A., Fischer, A., Bitzer, E., Bogusch, S., Beyer, T., van Straaten, H. W. and Viebahn, C. (2007). Ciliation and gene expression distinguish between node and posterior notochord in the mammalian embryo. *Differentiation* **75**, 133-146.

Blum, M., Beyer, T., Weber, T., Vick, P., Andre, P., Blitzer, E. and Schweickert, A. (2009). Xenopus, an ideal model system to study vertebrate left-right asymmetry. *Dev. Dyn.* **238**, 1215-1225.

Brennan, J., Norris, D. P. and Robertson, E. J. (2002). Nodal activity in the node governs left-right asymmetry. *Genes Dev.* **16**, 2339-2344.

Cartwright, J. H., Piro, O. and Tuval, I. (2004). Fluid-dynamical basis of the embryonic development of left-right asymmetry in vertebrates. *Proc. Natl. Acad. Sci. USA* **101**, 7234-7239.

Chicoine, J., Benoit, P., Gamberi, C., Paliouras, M., Simonelig, M. and Lasko, P. (2007). Bicaudal-C recruits CCR4-NOT deadenylase to target mRNAs and regulates oogenesis, cytoskeletal organization, and its own expression. *Dev. Cell* **13**, 691-704.

Cogswell, C., Price, S. J., Hou, X., Guay-Woodford, L. M., Flaherty, L. and Bryda, E. C. (2003). Positional cloning of jcpk/bpk locus of the mouse. *Mamm. Genome* **14**, 242-249.

Constam, D. B. and Robertson, E. J. (2000). SPC4/PACE4 regulates a TGFbeta signaling network during axis formation. *Genes Dev.* **14**, 1146-1155.

Corbit, K. C., Shyer, A. E., Dowdle, W. E., Gaulden, J., Singla, V., Chen, M. H., Chuang, P. T. and Reiter, J. F. (2008). Kif3a constrains beta-catenin-dependent Wnt signalling through dual ciliary and non-ciliary mechanisms. *Nat. Cell Biol.* **10**, 70-76.

Cougot, N., Babajko, S. and Seraphin, B. (2004). Cytoplasmic foci are sites of mRNA decay in human cells. *J. Cell Biol.* **165**, 31-40.

Eckmann, C. R., Kraemer, B., Wickens, M. and Kimble, J. (2002). GLD-3, a bicaudal-C homolog that inhibits FBF to control germline sex determination in C. elegans. *Dev. Cell* **3**, 697-710.

Eggenschwiler, J. T. and Anderson, K. V. (2007). Cilia and developmental signaling. *Annu. Rev. Cell Dev. Biol.* **23**, 345-373.

Essner, J. J., Vogan, K. J., Wagner, M. K., Tabin, C. J., Yost, H. J. and Brueckner, M. (2002). Conserved function for embryonic nodal cilia. *Nature* **418**, 37-38.

Etheridge, S. L., Ray, S., Li, S., Hamblet, N. S., Lijam, N., Tsang, M., Greer, J., Kardos, N., Wang, J., Sussman, D. J. et al. (2008). Murine dishevelled 3 functions in redundant pathways with dishevelled 1 and 2 in normal cardiac outflow tract, cochlea, and neural tube development. *PLoS Genet.* **4**, e1000259.

Eulalio, A., Behm-Ansmant, I. and Izaurralde, E. (2007). P bodies: at the crossroads of post-transcriptional pathways. *Nat. Rev. Mol. Cell Biol.* **8**, 9-22.

Feiguin, F., Hannus, M., Mlodzik, M. and Eaton, S. (2001). The ankyrin repeat protein Diego mediates Frizzled-dependent planar polarization. *Dev. Cell* **1**, 93-101.

Fischer, E., Legue, E., Doyen, A., Nato, F., Nicolas, J. F., Torres, V., Yaniv, M. and Pontoglio, M. (2006). Defective planar cell polarity in polycystic kidney disease. *Nat. Genet.* **38**, 21-23.

Gerdes, J. M., Liu, Y., Zaghloul, N. A., Leitch, C. C., Lawson, S. S., Kato, M., Beachy, P. A., Beales, P. L., Demartino, G. N., Fisher, S. et al. (2007). Disruption of the basal body compromises proteasomal function and perturbs intracellular Wnt response. *Nat. Genet.* **39**, 1350-1360.

Gerdes, J. M., Davis, E. E. and Katsanis, N. (2009). The vertebrate primary cilium in development, homeostasis, and disease. *Cell* **137**, 32-45.

Germino, G. G. (2005). Linking cilia to Wnts. *Nat. Genet.* **37**, 455-457.

Guay-Woodford, L. M. (2003). Murine models of polycystic kidney disease: molecular and therapeutic insights. *Am. J. Physiol. Renal Physiol.* **285**, F1034-F1049.
Hirokawa, N., Tanaka, Y., Okada, Y. and Takeda, S. (2006). Nodal flow and the generation of left-right asymmetry. *Cell* **125**, 33-45.
Hobbs, S., Jitrapakdee, S. and Wallace, J. C. (1998). Development of a bicistronic vector driven by the human polypeptide chain elongation factor 1alpha promoter for creation of stable mammalian cell lines that express very high levels of recombinant proteins. *Biochem. Biophys. Res. Commun.* **252**, 368-372.
Jones, C., Roper, V. C., Foucher, I., Qian, D., Banizs, B., Petit, C., Yoder, B. K. and Chen, P. (2008). Ciliary proteins link basal body polarization to planar cell polarity regulation. *Nat. Genet.* **40**, 69-77.
Kikuchi, A., Yamamoto, H. and Sato, A. (2009). Selective activation mechanisms of Wnt signaling pathways. *Trends Cell Biol.* **19**, 119-129.
Kishimoto, N., Cao, Y., Park, A. and Sun, Z. (2008). Cystic kidney gene seahorse regulates cilia-mediated processes and Wnt pathways. *Dev. Cell* **14**, 954-961.
Korinek, V., Barker, N., Morin, P. J., van Wichen, D., de Weger, R., Kinzler, K. W., Vogelstein, B. and Clevers, H. (1997). Constitutive transcriptional activation by a beta-catenin-Tcf complex in APC$^{-/-}$ colon carcinoma. *Science* **275**, 1784-1787.
Krebs, L. T., Iwai, N., Nonaka, S., Welsh, I. C., Lan, Y., Jiang, R., Saijoh, Y., O'Brien, T. P., Hamada, H. and Gridley, T. (2003). Notch signaling regulates left-right asymmetry determination by inducing Nodal expression. *Genes Dev.* **17**, 1207-1212.
Kugler, J. M., Chicoine, J. and Lasko, P. (2009). Bicaudal-C associates with a Trailer Hitch/Me31B complex and is required for efficient Gurken secretion. *Dev. Biol.* **328**, 160-172.
Levin, M., Johnson, R. L., Stern, C. D., Kuehn, M. and Tabin, C. (1995). A molecular pathway determining left-right asymmetry in chick embryogenesis. *Cell* **82**, 803-814.
Lin, M. D., Fan, S. J., Hsu, W. S. and Chou, T. B. (2006). Drosophila decapping protein 1, dDcp1, is a component of the oskar mRNP complex and directs its posterior localization in the oocyte. *Dev. Cell* **10**, 601-613.
Mahone, M., Saffman, E. E. and Lasko, P. F. (1995). Localized Bicaudal-C RNA encodes a protein containing a KH domain, the RNA binding motif of FMR1. *EMBO J.* **14**, 2043-2055.
Maretto, S., Cordenonsi, M., Dupont, S., Braghetta, P., Broccoli, V., Hassan, A. B., Volpin, D., Bressan, G. M. and Piccolo, S. (2003). Mapping Wnt/beta-catenin signaling during mouse development and in colorectal tumors. *Proc. Natl. Acad. Sci. USA* **100**, 3299-3304.
Mitchell, B., Stubbs, J. L., Huisman, F., Taborek, P., Yu, C. and Kintner, C. (2009). The PCP pathway instructs the planar orientation of ciliated cells in the Xenopus larval skin. *Curr. Biol.* **19**, 924-929.
Mochizuki, T., Saijoh, Y., Tsuchiya, K., Shirayoshi, Y., Takai, S., Taya, C., Yonekawa, H., Yamada, K., Nihei, H., Nakatsuji, N. et al. (1998). Cloning of inv, a gene that controls left/right asymmetry and kidney development. *Nature* **395**, 177-181.
Moeller, H., Jenny, A., Schaeffer, H. J., Schwarz-Romond, T., Mlodzik, M., Hammerschmidt, M. and Birchmeier, W. (2006). Diversin regulates heart formation and gastrulation movements in development. *Proc. Natl. Acad. Sci. USA* **103**, 15900-15905.
Morgan, D., Turnpenny, L., Goodship, J., Dai, W., Majumder, K., Matthews, L., Gardner, A., Schuster, G., Vien, L., Harrison, W. et al. (1998). Inversin, a novel gene in the vertebrate left-right axis pathway, is partially deleted in the inv mouse. *Nat. Genet.* **20**, 149-156.
Nakamura, T., Mine, N., Nakaguchi, E., Mochizuki, A., Yamamoto, M., Yashiro, K., Meno, C. and Hamada, H. (2006). Generation of robust left-right asymmetry in the mouse embryo requires a self-enhancement and lateral-inhibition system. *Dev. Cell* **11**, 495-504.
Nonaka, S., Tanaka, Y., Okada, Y., Takeda, S., Harada, A., Kanai, Y., Kido, M. and Hirokawa, N. (1998). Randomization of left-right asymmetry due to loss of nodal cilia generating leftward flow of extraembryonic fluid in mice lacking KIF3B motor protein. *Cell* **95**, 829-837.
Nonaka, S., Shiratori, H., Saijoh, Y. and Hamada, H. (2002). Determination of left-right patterning of the mouse embryo by artificial nodal flow. *Nature* **418**, 96-99.
Nonaka, S., Yoshiba, S., Watanabe, D., Ikeuchi, S., Goto, T., Marshall, W. F. and Hamada, H. (2005). De novo formation of left-right asymmetry by posterior tilt of nodal cilia. *PLoS Biol.* **3**, e268.
Okada, Y., Nonaka, S., Tanaka, Y., Saijoh, Y., Hamada, H. and Hirokawa, N. (1999). Abnormal nodal flow precedes situs inversus in iv and inv mice. *Mol. Cell* **4**, 459-468.
Okada, Y., Takeda, S., Tanaka, Y., Belmonte, J. C. and Hirokawa, N. (2005). Mechanism of nodal flow: a conserved symmetry breaking event in left-right axis determination. *Cell* **121**, 633-644.
Otto, E. A., Schermer, B., Obara, T., O'Toole, J. F., Hiller, K. S., Mueller, A. M., Ruf, R. G., Hoefele, J., Beekmann, F., Landau, D. et al. (2003). Mutations in INVS encoding inversin cause nephronophthisis type 2, linking renal cystic disease to the function of primary cilia and left-right axis determination. *Nat. Genet.* **34**, 413-420.
Park, T. J., Haigo, S. L. and Wallingford, J. B. (2006). Ciliogenesis defects in embryos lacking inturned or fuzzy function are associated with failure of planar cell polarity and Hedgehog signaling. *Nat. Genet.* **38**, 303-311.
Park, T. J., Mitchell, B. J., Abitua, P. B., Kintner, C. and Wallingford, J. B. (2008). Dishevelled controls apical docking and planar polarization of basal bodies in ciliated epithelial cells. *Nat. Genet.* **40**, 871-879.
Praetorius, H. A. and Spring, K. R. (2003). The renal cell primary cilium functions as a flow sensor. *Curr. Opin. Nephrol. Hypertens.* **12**, 517-520.
Qian, C. N., Knol, J., Igarashi, P., Lin, F., Zylstra, U., Teh, B. T. and Williams, B. O. (2005). Cystic renal neoplasia following conditional inactivation of apc in mouse renal tubular epithelium. *J. Biol. Chem.* **280**, 3938-3945.
Raya, A., Kawakami, Y., Rodriguez-Esteban, C., Buscher, D., Koth, C. M., Itoh, T., Morita, M., Raya, R. M., Dubova, I., Bessa, J. G. et al. (2003). Notch activity induces Nodal expression and mediates the establishment of left-right asymmetry in vertebrate embryos. *Genes Dev.* **17**, 1213-1218.
Saadi-Kheddouci, S., Berrebi, D., Romagnolo, B., Cluzeaud, F., Peuchmaur, M., Kahn, A., Vandewalle, A. and Perret, C. (2001). Early development of polycystic kidney disease in transgenic mice expressing an activated mutant of the beta-catenin gene. *Oncogene* **20**, 5972-5981.
Saburi, S., Hester, I., Fischer, E., Pontoglio, M., Eremina, V., Gessler, M., Quaggin, S. E., Harrison, R., Mount, R. and McNeill, H. (2008). Loss of Fat4 disrupts PCP signaling and oriented cell division and leads to cystic kidney disease. *Nat. Genet.* **40**, 1010-1015.
Saffman, E. E., Styhler, S., Rother, K., Li, W., Richard, S. and Lasko, P. (1998). Premature translation of oskar in oocytes lacking the RNA-binding protein bicaudal-C. *Mol. Cell. Biol.* **18**, 4855-4862.
Salzman, D. W., Shubert-Coleman, J. and Furneaux, H. (2007). P68 RNA helicase unwinds the human let-7 microRNA precursor duplex and is required for let-7-directed silencing of gene expression. *J. Biol. Chem.* **282**, 32773-32779.
Sbalzarini, I. F. and Koumoutsakos, P. (2005). Feature point tracking and trajectory analysis for video imaging in cell biology. *J. Struct. Biol.* **151**, 182-195.
Schwarz-Romond, T., Asbrand, C., Bakkers, J., Kuhl, M., Schaeffer, H. J., Huelsken, J., Behrens, J., Hammerschmidt, M. and Birchmeier, W. (2002). The ankyrin repeat protein Diversin recruits Casein kinase Iepsilon to the beta-catenin degradation complex and acts in both canonical Wnt and Wnt/JNK signaling. *Genes Dev.* **16**, 2073-2084.
Schwarz-Romond, T., Merrifield, C., Nichols, B. J. and Bienz, M. (2005). The Wnt signalling effector Dishevelled forms dynamic protein assemblies rather than stable associations with cytoplasmic vesicles. *J. Cell Sci.* **118**, 5269-5277.
Schwarz-Romond, T., Fiedler, M., Shibata, N., Butler, P. J., Kikuchi, A., Higuchi, Y. and Bienz, M. (2007a). The DIX domain of Dishevelled confers Wnt signaling by dynamic polymerization. *Nat. Struct. Mol. Biol.* **14**, 484-492.
Schwarz-Romond, T., Metcalfe, C. and Bienz, M. (2007b). Dynamic recruitment of axin by Dishevelled protein assemblies. *J. Cell Sci.* **120**, 2402-2412.
Schweickert, A., Weber, T., Beyer, T., Vick, P., Bogusch, S., Feistel, K. and Blum, M. (2007). Cilia-driven leftward flow determines laterality in Xenopus. *Curr. Biol.* **17**, 60-66.
Shiratori, H. and Hamada, H. (2006). The left-right axis in the mouse: from origin to morphology. *Development* **133**, 2095-2104.
Simons, M. and Mlodzik, M. (2008). Planar cell polarity signaling: from fly development to human disease. *Annu. Rev. Genet.* **42**, 517-540.
Simons, M., Gloy, J., Ganner, A., Bullerkotte, A., Bashkurov, M., Kronig, C., Schermer, B., Benzing, T., Cabello, O. A., Jenny, A. et al. (2005). Inversin, the gene product mutated in nephronophthisis type II, functions as a molecular switch between Wnt signaling pathways. *Nat. Genet.* **37**, 537-543.
Simons, M., Gault, W. J., Gotthardt, D., Rohatgi, R., Klein, T. J., Shao, Y., Lee, H. J., Wu, A. L., Fang, Y., Satlin, L. M. et al. (2009). Electrochemical cues regulate assembly of the Frizzled/Dishevelled complex at the plasma membrane during planar epithelial polarization. *Nat. Cell Biol.* **11**, 286-294.
Snee, M. J. and Macdonald, P. M. (2009). Bicaudal C and trailer hitch have similar roles in gurken mRNA localization and cytoskeletal organization. *Dev. Biol.* **328**, 434-444.
Tran, U., Pickney, L. M., Ozpolat, B. D. and Wessely, O. (2007). Xenopus Bicaudal-C is required for the differentiation of the amphibian pronephros. *Dev. Biol.* **307**, 152-164.
Wallingford, J. B. and Harland, R. M. (2002). Neural tube closure requires Dishevelled-dependent convergent extension of the midline. *Development* **129**, 5815-5825.
Wallingford, J. B. and Habas, R. (2005). The developmental biology of Dishevelled: an enigmatic protein governing cell fate and cell polarity. *Development* **132**, 4421-4436.
Wang, J., Hamblet, N. S., Mark, S., Dickinson, M. E., Brinkman, B. C., Segil, N., Fraser, S. E., Chen, P., Wallingford, J. B. and Wynshaw-Boris, A. (2006a). Dishevelled genes mediate a conserved mammalian PCP pathway to regulate convergent extension during neurulation. *Development* **133**, 1767-1778.
Wang, Y., Guo, N. and Nathans, J. (2006b). The role of Frizzled3 and Frizzled6 in neural tube closure and in the planar polarity of inner-ear sensory hair cells. *J. Neurosci.* **26**, 2147-2156.

Watanabe, D., Saijoh, Y., Nonaka, S., Sasaki, G., Ikawa, Y., Yokoyama, T. and Hamada, H. (2003). The left-right determinant Inversin is a component of node monocilia and other 9+0 cilia. *Development* **130**, 1725-1734.
Wessely, O., Tran, U., Zakin, L. and De Robertis, E. M. (2001). Identification and expression of the mammalian homologue of Bicaudal-C. *Mech. Dev.* **101**, 267-270.
Wilson, P. D. (2004). Polycystic kidney disease. *New Engl. J. Med.* **350**, 151-164.
Yamamoto, H., Komekado, H. and Kikuchi, A. (2006). Caveolin is necessary for Wnt-3a-dependent internalization of LRP6 and accumulation of beta-catenin. *Dev. Cell* **11**, 213-223.
Yang, L., Lin, C. and Liu, Z. R. (2006). P68 RNA helicase mediates PDGF-induced epithelial mesenchymal transition by displacing Axin from beta-catenin. *Cell* **127**, 139-155.
Yokoyama, T., Copeland, N. G., Jenkins, N. A., Montgomery, C. A., Elder, F. F. and Overbeek, P. A. (1993). Reversal of left-right asymmetry: a situs inversus mutation. *Science* **260**, 679-682.
Zheng, D., Ezzeddine, N., Chen, C. Y., Zhu, W., He, X. and Shyu, A. B. (2008). Deadenylation is prerequisite for P-body formation and mRNA decay in mammalian cells. *J. Cell Biol.* **182**, 89-101.